

January 01, 2007

Low temperature growth of crystalline magnesium oxide on hexagonal silicon carbide (0001) by molecular beam epitaxy

Trevor L. Goodrich

Northeastern University - Dept. of Chemical Engineering

J. Parisi

Northeastern University - Dept. of Chemical Engineering

Zhuhua Cai

Northeastern University - Dept. of Chemical Engineering

Katherine S. Ziemer

Northeastern University - Dept. of Chemical Engineering

Recommended Citation

Goodrich, Trevor L.; Parisi, J.; Cai, Zhuhua; and Ziemer, Katherine S., "Low temperature growth of crystalline magnesium oxide on hexagonal silicon carbide (0001) by molecular beam epitaxy" (2007). *Chemical Engineering Faculty Publications*. Paper 6.
<http://hdl.handle.net/2047/d20000711>

Low temperature growth of crystalline magnesium oxide on hexagonal silicon carbide (0001) by molecular beam epitaxy

T. L. Goodrich, J. Parisi, Z. Cai, and K. S. Ziemer^{a)}

Department of Chemical Engineering, Northeastern University, Boston, Massachusetts 02115

(Received 8 November 2006; accepted 2 January 2007; published online 25 January 2007)

Magnesium oxide (111) was grown epitaxially on hexagonal silicon carbide (6H-SiC) (0001) substrates at low temperatures by molecular beam epitaxy and a remote oxygen plasma source. The films were characterized by reflection high-energy electron diffraction, Auger electron spectroscopy, x-ray photoelectron spectroscopy, and atomic force microscopy. Crystal structure, morphology, and growth rate of the magnesium oxide (MgO) films were found to be dependent on the magnesium flux, indicating a magnesium adsorption controlled growth mechanism. The single crystalline MgO thin films had an epitaxial relationship where MgO (111) || 6H-SiC (0001) and were stable in both air and 10^{-9} Torr up to 1023 K. © 2007 American Institute of Physics. [DOI: 10.1063/1.2436636]

There is a growing need for the integration of complex functional oxides on semiconductors, particularly wide band gap semiconductors, for next generation, high-power, high-frequency, high-temperature, robust devices.¹ Some examples include the integration of magnetic barium hexaferrite ($\text{BaFe}_{12}\text{O}_{19}$) on silicon carbide (SiC) for self-biasing, robust microwave frequency devices,² or integration of lead zirconate titanate ($\text{Pb}(\text{Zr}_x\text{Ti}_{1-x})\text{O}_3$) on 6H-SiC as a tunable ferroelectric layer.^{3,4} The atomic arrangement of magnesium oxide (111) forms alternating layers of magnesium and oxygen in a quasihexagonal structure, similar to the hexagonal structure of 6H-SiC (0001). This suggests the possibility of a magnesium oxide (MgO) interface between the 6H-SiC substrate and the functional oxide film to alleviate lattice strain without interfering with any desired interaction between the functional films and the substrate. While there is limited literature of MgO film deposition by molecular beam epitaxy (MBE), Niu *et al.*⁵ reported using metal organic molecular beam epitaxy to epitaxially grow crystalline MgO (001) on silicon (001) with a 200 nm thick interlayer of crystalline 3C-SiC (001). Yadivalli *et al.*⁶ reported homoepitaxial growth of MgO (001) using MBE. More recently, Craft *et al.*⁷ demonstrated epitaxial MgO (111) on gallium nitride (0002). This letter reports the conformal, two-dimensional (2D) growth of crystalline, thermally stable MgO 20 Å thick on 6H-SiC by MBE as a potential template for films of more complex functional oxides.

After a standard degrease, 6H-SiC (0001) (Intrinsic Semiconductor) substrates were loaded into a custom built, hydrogen-flow furnace, based on the design by Ramachandran *et al.*⁸ and described elsewhere,⁹ in order to remove oxygen contamination and scratches due to polishing. Substrates were then immediately introduced to the ultrahigh vacuum (UHV) analysis chamber and evacuated to a base pressure of 1×10^{-9} Torr. Morphological studies of hydrogen etched substrates confirmed the removal of scratches and the formation of atomic steps similar to those reported in literature^{8,10} with a final root-mean-square (rms) roughness of 0.44 ± 0.03 nm, including the atomic steps. X-ray photoelectron spectroscopy (XPS) and Auger electron spectroscopy (AES) confirmed a clean, reproducible starting surface.

The UHV system used consists of an interconnected analysis chamber and an oxide growth chamber that allows chemical analysis of films without breaking vacuum after deposition. A PHI 10-360-4-015 hemispherical analyzer and PHI 04-173-0-077 Mg/Al dual anode nonmonochromated x-ray source was used for XPS, and a PHI 15-110B single pass cylindrical mirror analyzer was used for AES. XPS peak processing was performed using a full width at half maximum of 1.4 eV with an 80% Gaussian and 20% Lorentzian peak shape, as determined from a clean $\text{Au}4f_{7/2}$ photoelectron peak. Magnesium flux was supplied by a SPECS Scientific Instruments dual source, low-temperature, effusion cell using magnesium shavings (99.98%, Alpha Aesar). A remote oxygen rf-plasma source (Oxford Applied Research model HD25) provided atomic and molecular oxygen. Film growth was monitored with reflection high-energy electron diffraction (RHEED), consisting of a Staib Instruments RHEED system RH-15 and a k-Space Associates KSA 400 digital camera and software. Morphology was examined *ex situ* on a NANOPROBE IIIA Digital Instruments atomic force microscope (AFM) in contact mode with an oxide sharpened silicon nitride tip with a radius less than 20 nm.

For all experiments, the substrate temperature was held constant at 150 °C, as monitored using a type K thermocouple secured on the back of the molybdenum substrate holder. Calibration of the thermocouple using both a single and two-color pyrometer suggests an actual front face temperature of ~ 140 °C. The oxygen plasma was held constant at 100 W and a chamber pressure of 5×10^{-6} Torr, which correlates to an equivalent molecular oxygen flux of $1.8 \times 10^{15}/\text{cm}^2 \text{ s}$. This flux contains both O atoms and O_2 species (filtered 844 nm photomultiplier reading of 32 mV), but ion deflection plates located at the remote plasma discharge into the chamber prevented charged oxygen species from impinging on the substrate surface. Although actual atomic oxygen (versus molecular oxygen) flux has not been fully characterized due to equipment limitations, the absence of charged species was confirmed using a Hiden Analytical HALO 201 quadrupole mass spectrometer by setting the ionization energy to zero.

With the oxygen flux held constant, the magnesium flux was varied to study the influence of gas-phase magnesium to total oxygen (designated Mg:O) ratios on the nucleation and

^{a)}Electronic mail: kziemer@coe.neu.edu

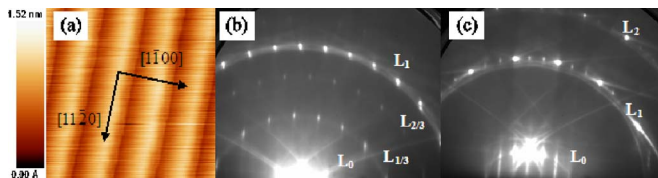


FIG. 1. Morphological and crystallographic characterizations of $6H$ -SiC (0001) by AFM and RHEED after *ex situ* hydrogen cleaning; (a) $1 \mu\text{m}^2$ AFM scan showing atomic steps that form along the $\{11\bar{2}0\}$ direction with a rms roughness of 0.44 nm; RHEED pattern showing a sharp $\sqrt{3} \times \sqrt{3}$ R30° surface reconstruction pattern with electron incidence along (b) $[11\bar{2}0]$ azimuth and (c) $[1\bar{1}00]$ azimuth.

growth mechanisms of MgO film formation. The Mg:O flux ratios were varied from 1:99, 1:49, 1:30, and 1:20 while the magnesium fluence was held constant at approximately $1.5 \times 10^{17}/\text{cm}^2$.

AFM results of hydrogen-cleaned substrates show distinct atomic steps for the $6H$ -SiC (0001), illustrated in Fig. 1. The $1 \mu\text{m}^2$ scan containing the atomic steps has a rms roughness of 0.44 ± 0.03 nm, an average step width of 265 ± 10 nm, and an average step height of 1.4 ± 0.2 nm. RHEED patterns show a sharp $\sqrt{3} \times \sqrt{3}$ R30° pattern.¹¹ XPS and AES analyses confirmed that the residual carbon contamination was removed during hydrogen cleaning. Remaining oxygen is approximately 1 ML silicate with a stoichiometry of $\text{Si}_2\text{O}_{2.8}$, similar to the findings of Bernhardt *et al.*¹⁰

When the Mg:O flux ratio was 1:49 and higher [Figs. 2(b)–2(d)], single crystalline MgO thin films exhibited a

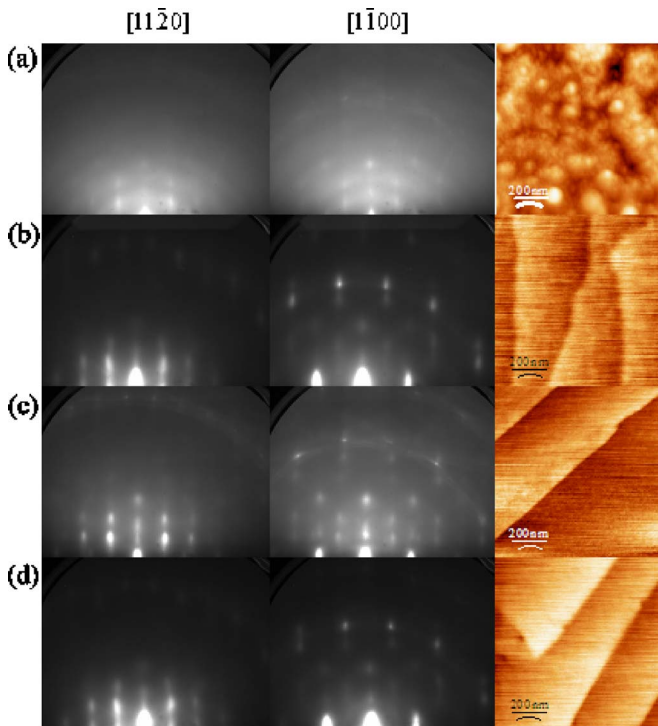


FIG. 2. RHEED patterns and AFM scans of 20 Å MgO thin films grown on $6H$ -SiC (0001) at different Mg:O flux ratios; (a) 1:99, (b) 1:49, (c) 1:30, and (d) 1:20. Left column corresponds to an incidence along the $[11\bar{2}0]$ azimuth for bulk $6H$ -SiC, which correlates to an incidence along the $[1\bar{1}0]$ for MgO (111). Center column corresponds to an incidence along the $[1\bar{1}00]$ azimuth for $6H$ -SiC, which correlates to an incidence along the $[11\bar{2}]$ for MgO (111). The right column corresponds to $1 \mu\text{m}^2$ AFM scans with rms values of 2.8, 0.23, 0.45, and 0.48 nm for (a)–(d), respectively.

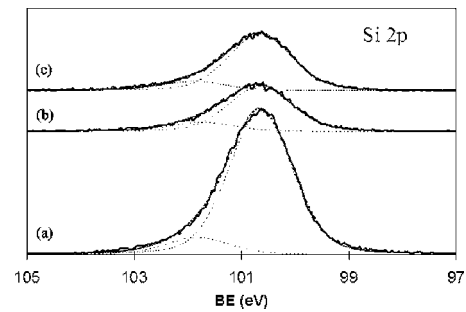


FIG. 3. XPS elemental scan of Si2p for (a) clean $6H$ -SiC, (b) 20 Å MgO on $6H$ -SiC, and (c) 20 Å MgO on $6H$ -SiC after annealing at 800 °C for 90 min. The consistency of the Si2p peak indicates that the MgO film is thermally stable without any diffusion at the interface.

MgO (111) RHEED pattern.¹² The resulting films were conformal to the substrate steps, and were smooth, with an average rms roughness of 0.39 ± 0.04 nm. However, when the magnesium flux was lowered to 1:99 [Fig. 2(a)], the RHEED pattern suggested polycrystallinity within the film, and AFM scans indicated a loss of conformal epitaxy with highly three-dimensional (3D) growth features and a rms roughness of 2.79 ± 0.20 nm.

The attenuated Si2p and C1s photoelectron peaks originating from the bulk $6H$ -SiC were used to estimate the MgO film thicknesses to 20 ± 2.5 Å using the TPP-2M and Gries equations.¹³ The growth rates increased fairly linearly with increased magnesium flux, indicating a magnesium adsorption controlled growth mechanism. The magnesium incorporation efficiency ranged from 12% to 38%. Note that these are approximate incorporation efficiencies because thickness is measured through attenuation of substrate peaks that gives a 10% error in calculated thicknesses. In addition, while all these samples were run within a few days so that they are comparable to each other, Mg flux is calculated from effusion cell temperature, so can drift over time.

The transition from a 2D single crystalline growth mechanism to a 3D polycrystalline growth mechanism, illustrated in Fig. 2(a), is hypothesized to be a result of over oxidizing the silicon terminated $6H$ -SiC causing a loss of crystallinity at the substrate surface which produced polycrystalline MgO. To test this hypothesis, clean $6H$ -SiC (0001) reconstructed to $\sqrt{3} \times \sqrt{3}$ R30° was intentionally oxidized for 60 min at 150 °C, 100 W, and a chamber pressure of 5×10^{-6} Torr. RHEED observations confirmed a decrease in crystallinity and the loss of the $\sqrt{3} \times \sqrt{3}$ R30° surface. XPS confirmed a surface oxygen concentration around 32%. Subsequent MgO growth was performed with conditions identical to Fig. 2(d). The resulting MgO film was highly polycrystalline. This suggests that the crystal structure and orientation of the MgO films may be highly dependent on the crystal quality of the substrate. Epitaxial growth of MgO is possible as long as the crystalline structure of the substrate is maintained during film nucleation and the initial stages of growth.

In order for the MgO films to be effective interfaces for subsequent complex oxide deposition, they need to be stable at temperatures ranging from 580 to 800 °C^{3,4} or even higher up to 1100 °C.² To test thermal stability, the 20 Å MgO films on $6H$ -SiC were heated rapidly (~ 5 min ramp) under vacuum to a calibrated front face temperature of approximately 750 °C. The sample was held at high temperature at 10^{-9} Torr for 90 min, then the current to the heater

was removed. XPS analysis of the Si2*p* and C1*s* peak was performed before MgO deposition, after 20 Å of MgO, and after heating. Based on the peak shape and deconvolution of the elemental spectra, there was no evidence of interfacial breakdown or interdiffusion. As the silicon peak would seem to be the most likely to show interface breakdown, Fig. 3 shows the Si2*p* peak stability. Thus, the thin, crystalline MgO can be an effective template for integrating more complex oxides on the wide band gap semiconductor, 6*H*-SiC.

In summary, we have demonstrated smooth, thermally stable, crystalline MgO thin films, 20±5 Å thick, grown at low temperatures on 6*H*-SiC (0001) through MBE. Growth conditions where the Mg:O flux ratio was 1:25 or higher resulted in single crystalline films that grew conformal to the 6*H*-SiC atomic steps with the epitaxial relationship MgO (111)∥6*H*-SiC (0001). Lower Mg:O flux ratios resulted in polycrystalline films with 3D growth features. The growth rate of the MgO films was found to increase linearly with increased magnesium flux, indicating a magnesium controlled growth mechanism and a magnesium incorporation efficiency around 8.0±1.8%.

This research was supported by Office of Naval Research under Contract Nos. N0014-06-1-0761 and N00014-04-1-0426, Colin Wood Program Monitor. The authors

would like to thank Al Sacco, Jr. at Northeastern University for use of the AFM.

- ¹W. A. Doolittle, A. G. Carver, and W. Henderson, *J. Vac. Sci. Technol. B* **23**, 1272 (2005).
- ²Z. Chen, A. Yang, S. D. Yoon, K. Ziemer, C. Vittoria, and V. G. Harris, *J. Magn. Magn. Mater.* **301**, 166 (2006).
- ³S. M. Koo, S. I. Khartsev, C. M. Zetterling, A. M. Grishiin, and M. Östling, *Appl. Phys. Lett.* **81**, 895 (2002).
- ⁴D. Mou, J. Linnros, C. S. Petersson, and K. V. Rao, *J. Appl. Phys.* **84**, 5785 (1998).
- ⁵F. Niu, B. H. Hoerman, and B. W. Wessels, *J. Vac. Sci. Technol. B* **18**, 2146 (2000).
- ⁶S. Yadivalli, M. H. Yang, and C. P. Flynn, *Phys. Rev. B* **41**, 7961 (1990).
- ⁷H. S. Craft, J. F. Ihlefeld, M. D. Losego, R. Collazo, Z. Sitar, and J.-P. Maria, *Appl. Phys. Lett.* **88**, 212906 (2006).
- ⁸V. Ramachandran, M. F. Brady, A. R. Smith, R. M. Feenstra, and D. W. Greve, *J. Electron. Mater.* **27**, 308 (1996).
- ⁹T. Goodrich, J. Parisi, J. Leong, and K. S. Ziemer, AICHE Annual Meeting Conference Proceedings 2005, Cincinnati, OH, 30 October–4 November 2005, pp. 135e/1–135e/5.
- ¹⁰J. Bernhardt, J. Schardt, U. Starke, and K. Heinz, *Appl. Phys. Lett.* **74**, 1084 (1999).
- ¹¹X. N. Xie and K. P. Loh, *Appl. Phys. Lett.* **77**, 3361 (2000).
- ¹²V. K. Lazarov, R. Plass, H.-C. Poon, D. K. Saldin, M. Weinert, S. A. Chambers, and M. Gajdardziska-Josifovska, *Phys. Rev. B* **71**, 115434 (2005).
- ¹³NIST Database 82, version 1.0, U. S. Department of Commerce (2001).